Available online at www.eccomasproceedia.org
Eccomas Proceedia COMPDYN (2019) 5802-5812

ECCOMAS
Proceedia

COMPDYN 2019
7th ECCOMAS Thematic Conference on
Computational Methods in Structural Dynamics and Earthquake Engineering
M. Papadrakakis, M. Fragiadakis (eds.)
Crete, Greece, 24–26 June 2019

EXPERIMENTAL AND NUMERICAL SIMULATIONS ON RBS CONNECTIONS INCORPORATING LARGE SECTIONS

T. Bogdan[1], D.V. Bompa[2], A.Y. Elghazouli[2], E. Nunez[3] M. Eatherthon[4], and R. Leon[4]

[1] ArcelorMittal Global Research and Development Esch, Esch sur Alzette, Luxembourg
e-mail: Teodora.bogdan@arcelormittal.com

[2] Department of Civil and Environmental Engineering, Imperial College London, UK
e-mails:d.bompa@imperial.ac.uk, a.elghazouli@imperial.ac.uk

[3] ArcelorMittal Global Research and Development Basque Country, Bilbao, Spain
e-mail: edurne.nunez@arcelormittal.com

[4] Via Department of Civil and Environmental Engineering, Virginia Tech, Blacksburg, USA
e-mail: meather@vt.edu; rleon@vt.edu

Abstract

Recent experimental tests have shown that RBS connections incorporating Jumbo specimens meet the current seismic design qualification protocols, allowing to further extend the current seismic provisions for prequalified steel connections with possible applications of heavy steel sections beyond their current use in ultra-tall buildings. The experimental results and observations described in this paper enabled a better understanding of the structural behaviour of RBS connections made of heavy structural sections for application in seismic regions. However, the results indicate that geometrical and material effects need to be carefully considered when designing welded RBS connections incorporating large steel profiles. To better interpret the experimental results, extensive detailed non-linear finite element simulations are conducted on the entire series of tests, comprising of three large-scale specimens with distinct sizes. The analyses intend to clarify the scale effects that influence the performance of these connections, both at material and geometric level, and particularly to understand the balance in deformation between the column panel zones and the reduced beam section and level of stress within the main connection components. It is shown that the numerical models for all three specimens reproduce accurately the overall load-deformation and moment-rotation time history.

Keywords: reduced beam sections; steel connections; welded connections; seismic design; non-linear modelling.

ISSN:2623-3347
Peer-review under responsibility of the organizing committee of COMPDYN 2019.
doi: 10.7712/120119.7346.19822

1 INTRODUCTION

Structural members with long uninterrupted spanning and large loading capacity are needed in the design of tall buildings, convention centres, sport arenas and airport concourses. The latest product developments made by ArcelorMittal permits the use of large jumbo steel profiles as W920x420x1377 (W36×925) with steel of 450 MPa in grades like S460 and HISTAR 460, available both on the US and European market. When such profiles are used in areas of high seismicity, the welded connection design requires a careful development from welding performance specifications (WPS) point to ensure that the required rotational capacities to reach interstudy drifts of 4% can be developed. One technique used to control the flexural demand from the beam is to utilize reduced beam sections (RBS), which effectively limit the demands at the beam-column interface (Figure 1).

The RBS concept was proposed initially by Plumier [1] in the late 1990s to alleviate problems encountered in the 1994 Northridge Earthquake with conventional welded connections. Following, different shapes of RBS have been studied along the time. For example, Iwankiw and Carter [2] studied the first polygonal cut and observed initial yielding in the column panel zone (PZ) followed by diagonal yield lines in the beam flanges. Englehart [3] observed that a higher performance goal might be achieved by changing the shape from constant to a radius cut dogbone. Moreover, Zekioglu et al [4] showed that the application of large plastic rotation capacities, without considering the strength degradation or rotation demand range, to justify a particular moment frame system, would not be a rational approach.

Popov et al. [5] showed in tests that the triaxial loading makes steel at a connection fail without exhibiting yielding ductile behaviour due to the state of stress and not because of material property. Later, Uang et al [6] used a database of 55 cyclically full-scale RBS moment connection tests to study the cyclic instability of such connections. They observed that the slenderness ratio for web local buckling affects the plastic rotation. Ultimately, Zhang and Ricles [7,8] investigated the RBS moment connections to a deep wide flange column and observed that thee composite floor can significantly reduce the lateral displacement of the beam bottom flange in the RBS and the amount of twist developed in the column.

The current AISC Provisions for Steel Buildings (AISC 360-16) [9], Seismic Provisions (AISC 341-16) [10] and the Provisions for Prequalified Connections for Special and Intermediate Steel Moment Frames (AISC 358-16) allow the use of these connections but only for sections up to 900 mm in depth and 450 kg/m in weight [11]. To extend the coverage of these specifications to much larger sections, a joint experimental and analytical program was undertaken by Virginia Tech and ArcelorMittal [12]. It is worth noting, that codified prequalification procedures for seismic steel connections are under development in Europe as a result of the recently completed Equaljoints research project [13].

In this paper, results and observations from an experimental program on three RBS connections provided with large section are reported. Complementary numerical studies are also undertaken using nonlinear finite element procedures which are validated against the experimental results from this study. Comparative assessments are also presented, including stiffness and strength as well as ductility and energy dissipation are examined.

2 EXPERIMENTAL AND NUMERICAL METHODOLOGY

2.1 Testing arrangement and specimen details

The experimental campaign is based on a trial design to determine the realistic member size in buildings with high seismicity area [12]. The study consisted of a square office building tower with fifteen stories and a large open atrium at the 1st floor. Special Moment Frames

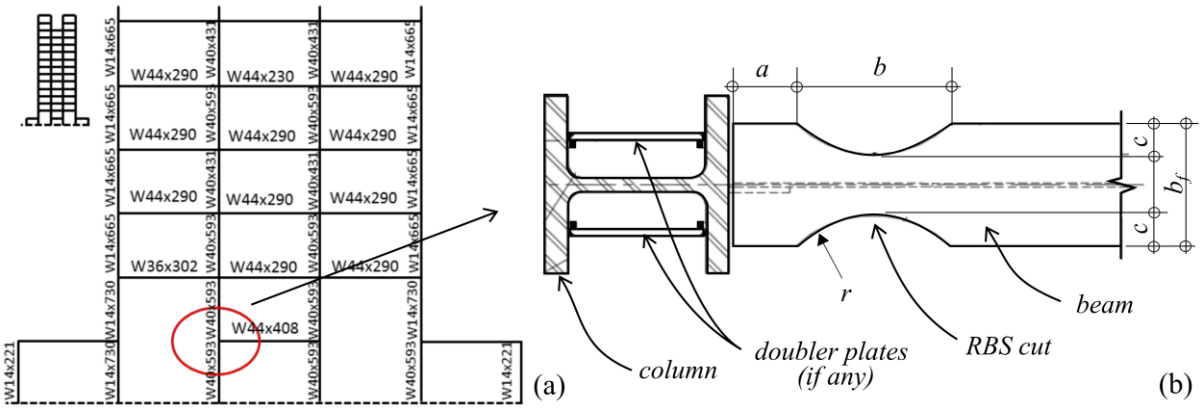

Figure 1: a) Sections at the lower storeys of the Case study building, b) Plan detail of the examined beam-column connections with doubler plates.

Spec.	Beam	Column	Doubler plate	RBS cut			Cont. plates
				A mm (in)	B mm (in)	C mm (in)	
SP2	W 44x408	W 14x873	None	200.5 (7.9)	708.5 (27.89)	68 (2.69)	None
SP3	W 36x925	W 14x873	5/8	236.5 (9.31)	710.5 (27.97)	99 (3.91)	None
SP4	W 44x408	W 40x503	None	305 (12.00)	950 (37.40)	85 (3.36)	None

Table 1: Specimen details

with RBS connections were considered exclusively for the seismic-load-resisting system. These frames are located at the perimeter and are typically three bays wide, except at the lower levels as shown in Figure 1a. From these typical frames, sample connections were extracted as possible test specimens. Table 1 presents the chosen configurations for the testing, whilst Figure 1b depicts the schematic of a specimen. Each specimen exceeds the size limitation outlined in the AISC 358-16 [11] in at least one regard.

The specimens were secured within a rigid frame that is affixed to the strong floor laboratory as illustrated in Figure 2 and the schematic representation in Figure 3a. The pieces in red indicates where the frame was being fixed to the strong floor. The frame connects to the strong floor in two different ways. The first set of connections to the strong floor is made up of eight stiffened W33×291 members. These eight members take load in the longitudinal direction (parallel to both the actuators and the W members embedded within the strong floor). Each of the members is secured to the W members embedded within the strong floor (depicted as grey strips in Figure 3a) with 42 × one-inch (25.4 mm) A490 bolts in slip-critical connection (achieved with pre-tensioning). The second set of connections to the strong floor involves two large steel wedge shape blocks, designed to take the load in the lateral direction.

As observed, the specimens were tested in the horizontal orientation in displacement control with the actuators reacting to the testing frame. The specimens were subjected to the loading protocol described in AISC 341-16 [10], as illustrated in Figure 3b. After two cycles at a story drift angle of 0.04 rad, the story drift increases by 0.01 rad increments every two cycles until failure. Due to stroke limitations in the actuators, the maximum achievable story drift during these tests was 0.06 rad, hence, the specimens were cycled at 0.06 rad until failure. Specimen instrumetation included a combination of linear and string potentiometers, strain gauges and rosettes, and an in-house imaging system (OJOS) in order to capture all pertinent measurements for analyzing the system as a whole. Results from these devices are later used for the numerical validation descriBed later.

Figure 2 Specimen in testing orientation with two actuators

Is is worth noting that besides the extension of prequalification limits in the AISC codes, another main objective of the experimental programme was to determine an acceptable balance between the deformation obtained from flexural yielding of the RBS and shear yielding of the column web PZ [12]

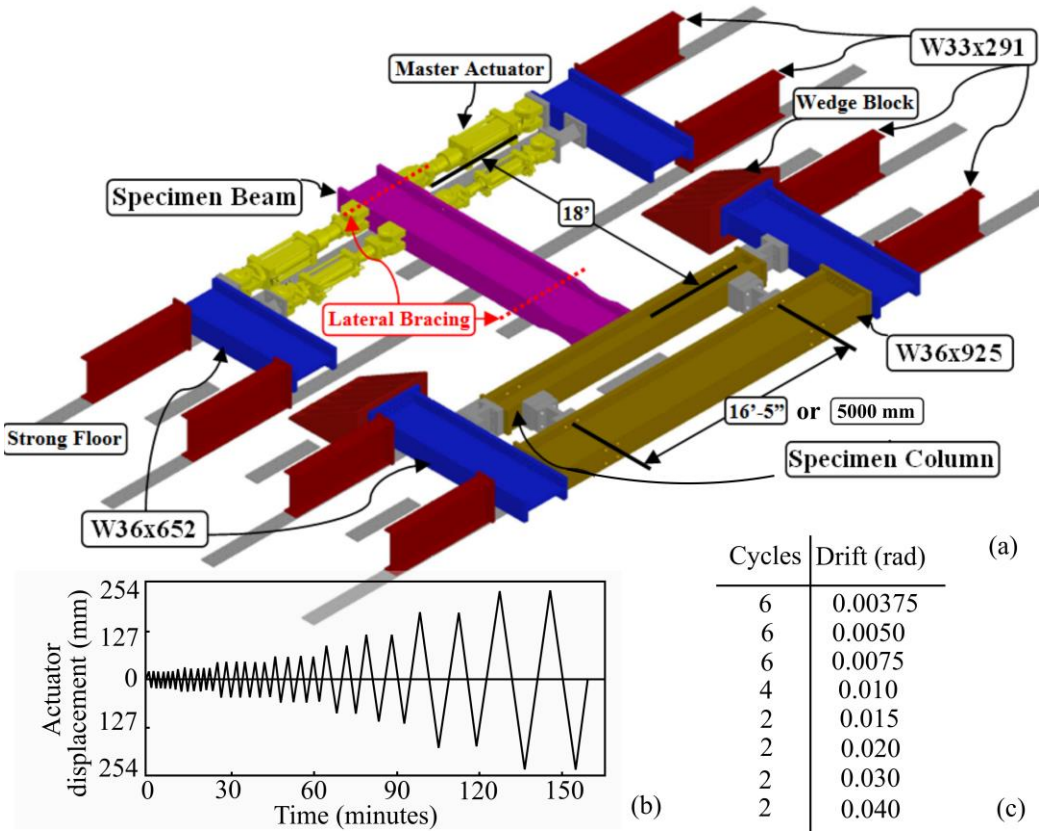

Figure 3 a) Test setup with four actuators, b) Loading protocol – AISC 2010..

2.2 Numerical procedures

The numerical simulations described in this paper were carried out using the non-linear finite element (FE) program ABAQUS [14]. Tri-dimensional (3D) models of RBS connections adopt eight node brick elements (C3D8R). Extruded solid elements from heavy W sections representing the column were connected to the beams using tie constraints. Special attention was given to the characteristics of the RBS region and the column PZ by considering the exact dimensions taken from the experimental specimens (Table 2). Initial studies indicated that the experimental stiffness of specimens with the largest cross-sections (SP3) differed from analytical assessments [12]. To address the potential influence from the test rig, two modelling approaches were considered. Firstly, the specimens, including the four stub elements made of W sections used as boundary conditions were modelled together. Multi-point constraints connected to reference points assigned with pinned boundary conditions to the exterior face of the W profile, whilst surface-to-surface interactions were assigned to the interface between the column element of the specimens and stub elements. Secondly, the specimens described in Section 2.1 were modelled along with the complete testing arrangement as illustrated in Figure 3a. Similarly, pinned boundary conditions were assigned to reference points that were connected through multi-points constraints to the rig elements. All contacts between specimens and rig elements were modelled using surface-to-surface interactions.

Cyclic displacements were applied to reference points that are connected to beam tips through constraints and transfer plates simulating firmly the experimental time history. Mesh sensitivity studies were undertaken assess the element size influence on the hysteretic response. These indicate that a relatively coarse mesh restricts a reliable inelastic strain propagation within the RBS and local buckling effects are not captured. On the other hand, a fine mesh within the RBS and column PZ ($l_m \approx$15-20 mm), combined with $l_m \approx$30-40 mm outside of the critical regions offer reliable deformations and strains, as described in the subsequent sections. A minimum of two mesh rows per flange thickness offer a good balance in terms of computational time and reliability of the results, whilst a much larger number of rows significantly increase the analysis time and reduce the ability of the model to capture local effects, primarily due to hourglass effects [15]. The Newton-Raphson approach was adopted for the numerical integration procedure. The steel material properties were modelled using a plastic multilinear kinematic hardening [14] constitutive representation in which the materials properties obtained from coupon testing, separately for webs and flanges, were accounted for. The yield strength varied between f_y=440-477 MPa and the ultimate strength varied between f_u=609-702 MPa.

3 TEST RESULTS AND NUMERICAL VALIDATION

A reliable failure mode of RBS connections is triggered by yielding at the RBS, followed by limited yielding of the PZ and ultimately local flange buckling at the RBS. The latter is an important mechanism as controls the connection behaviour acting as limit to hardening in flexurally governed yielding responses [12]. Close inspection on the slenderness parameters of the section showed that SP2 and SP4 were susceptible to such sequence of yielding and failure. As the slenderness of both web and flanges are relatively low for SP3, local buckling is unlikely to develop. As expected, SP2 and SP4, failed by flexural yielding and inelastic local buckling, and achieved the desired deformation capacity [12] as illustrated Figure 4a,c. The load-displacement curves for these specimens indicate typical, yielding post-buckling softening after maximum capacity was reached. In contrast, SP3, with significantly higher sections reached flexural yielding, failing relatively sudden without any evidence of softening (Figure 4b). This behaviour was attributed to the extreme demands on the very thick welds,

for which the conventional design procedures may substantially underestimate the local strain demands under cyclic displacements [12].

Non-linear numerical validation of the experimental results of Specimens SP2, SP3 and SP4 were undertaken by accounting for the procedures described in Section 2.2. Figures 4d-e present the relationship between load versus beam tip deflection of the above. The results indicate reliable prediction in terms of elastic stiffness, yielding characteristics, deformations and relatively good predictions of the hysteretic response for Specimen SP2. Remarkably, the model can closely capture the initiation of flange buckling and plastic development in the RBS region and PZ. It is worth noting that the numerical model of SP2 showed slightly larger deformations at RBS and slightly lower deformations at the PZ, recorded as displacement reaction from beam flanges in the column, in comparison to the test response.

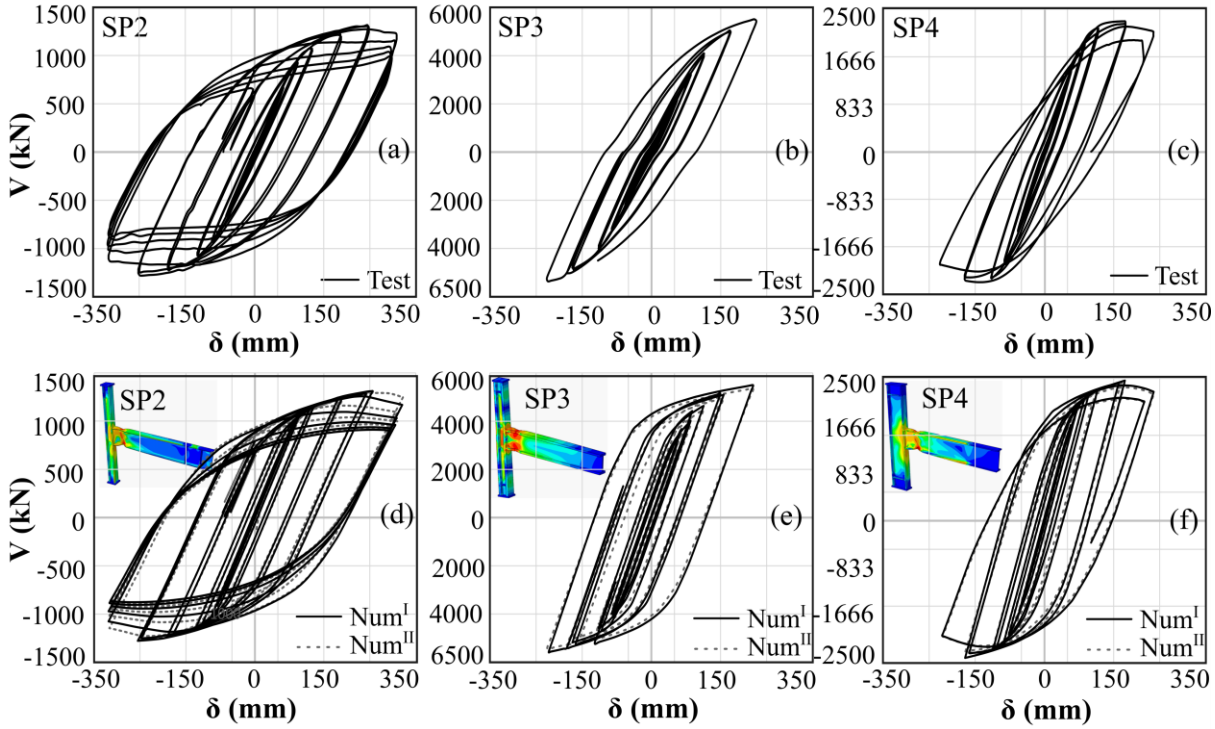

Figure 4: Test force – deflection (V-δ) a) SP2, b) SP3, c) SP4; Numerical validation d) SP2, e) SP3, f) SP4

On the other hand, the behaviour of SP3 was predicted well only in terms of capacity and corresponding displacement, with the numerical stiffness being more rigid in comparison to the experimental stiffness. The test load-displacement of SP3 shows some pinching and change in the unloading stiffness at load reversal, which is not captured with the adopted modelling approach, primarily since all connections between rig elements are modelled with tie constraints, whilst in tests these were rather discrete at the bolted connections. Simulation results of Specimen SP4 show good agreement in terms of stiffness, capacity and degradation, yet the energy dissipation, considered as the area enclosed under the hysteretic loops, is over-estimated. For this specimen the numerical displacements at RBS in tension is identical with the test response, whilst the compression is slightly over-estimated. This is however compensated by a decrease in the deformation at the PZ at which the numerical displacement is about 35% less than the test displacement (Figure 5).

The direct comparison between the models with and without testing rig allowed for an improved understanding of the rig compliance to the load-displacement response. Except the

post-buckling softening response, for SP2 and SP4, the test and numerical curves in Figures 4d,f are virtually identical in terms of key structural parameters and hysteretic response. For SP3, which had significantly larger section sizes in comparison to SP2 and SP4, there is some deviation in the elastic stiffness, primarily due to higher reactions at the boundary conditions of the specimen. Also, the numerical results indicated that the webs of the stub elements that connected the SP3 column to the reaction stubs developed inelastic strains. Additional modelling of the slip between elements fixed to the strong floor and connected rig elements, r by transducers, reduced the stiffness of SP3, being closer to the experimental stiffness, yet more rigid.

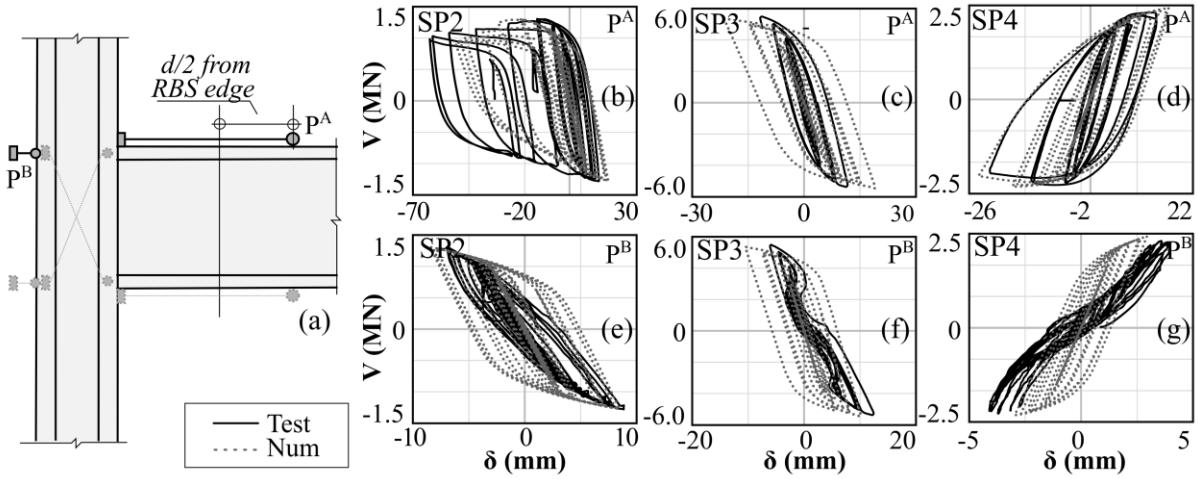

Figure 5 a) Instrumentation extract; Comparison of deformations at RBS b) SP2, c) SP3, d) SP4; at column flange due to force introduction from beam flanges e) SP2, f) SP3, g) SP4.

Observations from models indicate that although the welds were not explicitly modelled, the inelastic strain maps obtained from the SP3 model showed initiation of yielding in the beam at the column face and further in the web column panel, with lower stresses in the RBS flanges than in its web. Also, the direct comparison between the test hysteretic responses of SP2 and SP4 versus SP3 indicate a relatively distinct response. The latter depicts a less ductile behaviour with a lower amount of energy dissipated through the loops. These observations combined with test and numerical results from literature on RBS beam-to-column connections [5] with relatively large sections suggest a possible size effect in cyclic response of large size steel connections. As material models employed in numerical simulations are typically validated against tests on relatively small samples, at significant inelastic strains, these may not reliably represent the structural response when plastic strains develop on large areas.

4 COMPARATIVE ASSESSMENTS

This section describes a detailed analysis of the response of the connections investigated in terms of moment-rotation envelopes, ductility, energy dissipation and stiffness. Bending moments M were assessed at the face of the column from actuator loads in case of experiments and reaction forces at reference points for numerical models. For the global behaviour, chord rotations θ are assessed from beam tip displacements. Figure 6a depicts both test and numerical M-θ envelope curves determined from the V-δ from Figure 4. Besides M-θ curves, the yield moment M_y at the RBS, using assessed material strengths, for each specimen is presented. As observed, the yield moment, represented by a change in member stiffness for both test and numerical models intersects with the analytical assessments, marked with dashed lines.

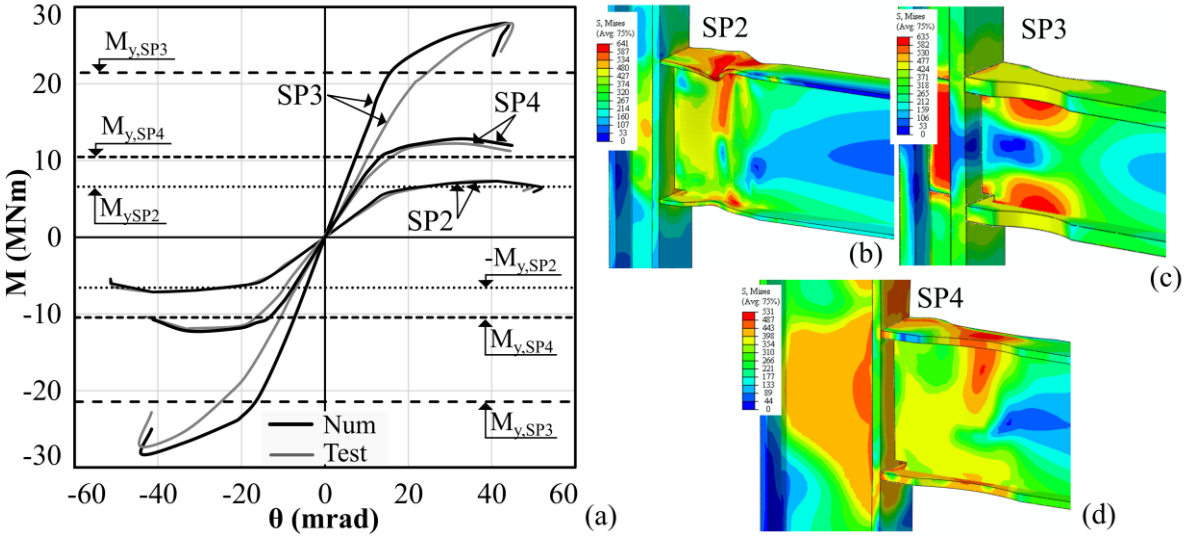

Figure 6 a) Moment – rotation envelopes; stress fields at peak displacement for b) SP2, c) SP3, d) SP4

All specimens exhibited acceptable levels of ductility at ultimate with values above 40 mrad. Specimens SP2 and SP4 had higher ductility and enhanced hysteretic response in comparison to SP3, as also described in previous sections. This is also highlighted by a direct comparison between the test and numerical M-θ curves. For SP2 and SP4 there is a very good agreement in terms of stiffness, yield moment M_y, hardening, ultimate moment M_u and softening. On the other hand, although the yield and capacity of SP3 are well captured by the numerical simulations, the test stiffness is lower than its numerical counterpart. It is worth noting that the size of SP3 was significantly higher than of the SP2 and SP4, hence the M_u at the column face for SP3 was in the range of 27.9 MNm, which is 2.3 × M_u of SP4 and 3.8 × M_u of SP2.

Figures 6b-d illustrate the Mises stress fields at the last cycle of the peak displacement applied. The stress distributions indicate (i) flange buckling at RBS for SP2 with a lower damage at the PZ (Figure 6b), (ii) concentration of stresses at PZ and beam web with lower stress levels at the RBS flanges at SP3 (Figure 6c), and (iii) non-symmetric stress distribution at RBS and PZ with out-of-plane column rotation for SP4 (Figure 6d). It is suggested that the cyclic degradation of SP2 resulted from buckling at the RBS, whilst at SP4 the initiation of buckling was combined with column twist and column web buckling. In contrast, as the RBS flanges of SP3 had lower stress levels than the remaining connection components, there was no degradation at RBS, yet significant column web panel distortion occurred.

The contributions of the RBS and column web PZ obtained from numerical simulations are depicted in Figures 7a-c. The rotation at RBS was assessed from the relative displacements of the top and bottom RBS cuts, and divided by the beam depths. The web column rotation was determined from the relative web displacements resulted from force induction by beam flanges and relative vertical panel displacements [16]. As indicated in the figure, SP2 an SP4, dissipated large energy proportions through the RBS, with the PZ contributing in the range of 15-25%; hence a stronger PZ. On the other hand, SP3 had a relatively even contribution of the two components indicating a relatively balanced behaviour. A close inspection on an identical model of SP3 without double plates showed a contribution of the web column panel of about 70% to the connection rotation, resulting in excessive distortional demands leading to unreliable performance of the components [17,18].

Figures 7d-e indicate the cumulative energy dissipation, integrated from the hysteretic loops converted in M-θ from Figure 4, and the decrease in secant stiffness in relation with θ. As described before, SP2 had stable hysteretic loops and a ductile response with θ_u=50.5 mrad. This is captured by the cumulative energy curve whose stiffness increases with rotation. Additionally, as the numerical response was in good agreement with the test curves, the test and numerical E_d curves of SP2 nearly overlap. On the other hand, SP3 and SP4 reached lower E_d indicating poorer hysteretic response in comparison to SP2 yet reaching reliable ductility levels (θ_u≈mrad). More importantly, considering that the yield rotation was around θ_y=15 mrad for all members, the plastic rotation θ_p=30-35 mrad indicating that these connections developed reliable response for connections in seismic resistant structures with θ_p being between the minimum requirements for ductility class medium ($\theta_{p,M}$=25 mrad) and for ductility class high ($\theta_{p,M}$=35 mrad) [19].

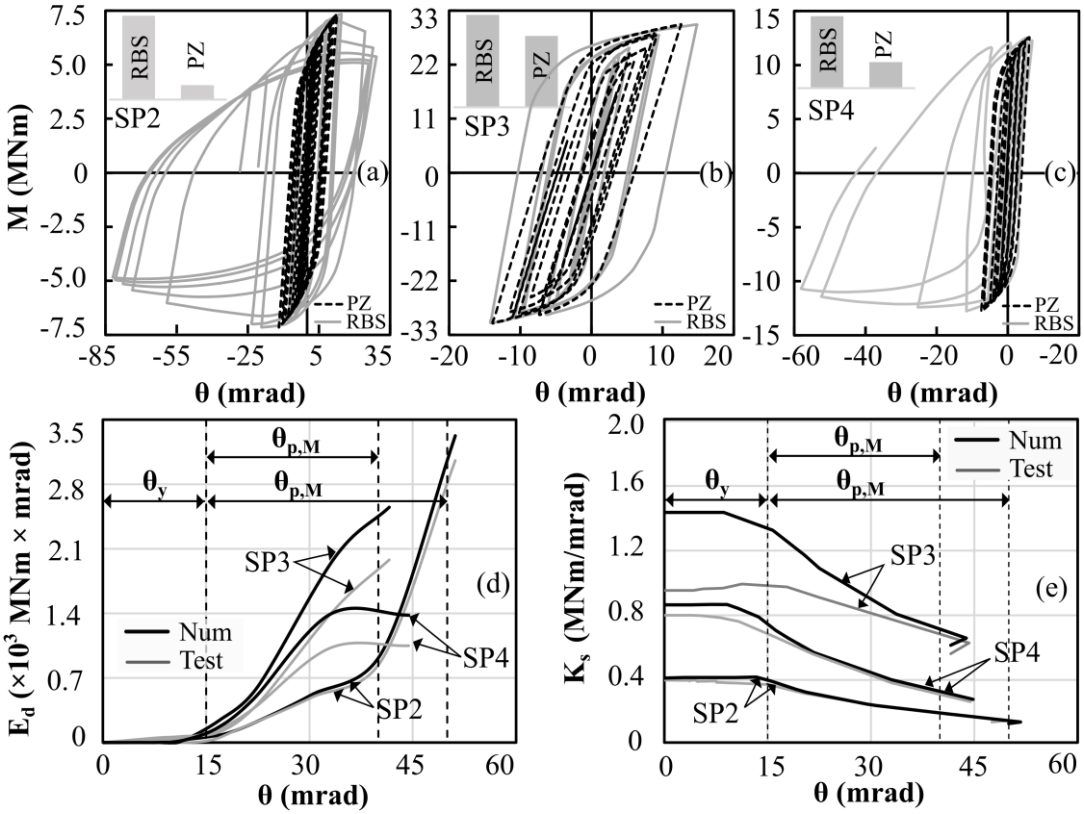

Figure 7 Contribution of connection components for Specimen a) SP2, b) SP3, c) SP4; d) Cumulative energy dissipation versus rotation; e) Stiffness versus rotation

5 CONCLUSIONS

The performance of reduced beam section (RBS) beam-to-column connections incorporating large jumbo steel profiles subjected to cyclic loading was investigated in this study. The experimental and numerical results showed that the strength, stiffness, ductility, hysteretic response and failure mode of such connections are largely dependent on the beam and column section sizes. The results indicated that RBS beam sections with relatively high depth-to-web thickness slenderness ratios develop reliable failure modes characterised by extensive yielding at the RBS, followed by yielding at the panel zone (PZ) and ultimately, flange buckling at RBS. Also, for relatively deep columns, force induction from beam flanges, combined with RBS flange buckling, could produce out-of-plane column rotation. These connections

developed responses characterised by stable hysteretic response, a relatively strong PZ and reliable ductility levels.

In contrast, compact sections with relatively low depth-to-web thickness ratios may develop unreliable response with yielding developing almost concomitantly and at RBS and PZ, having a relatively equal contribution to the total connection deformation. Numerical simulations showed that for connections with relatively compact sections, a higher concentration of stresses may occur at the PZ and at the beam, web with lower stress levels developing at the RBS flanges. These observations indicate the need for an alternative design procedure of RBS for connections incorporating large compact sections. More importantly, the connections investigated in this paper reached reliable rotational capacities, that correspond to inter-story drifts of 4% as a minimum required by North American prequalification standards. This corresponds to plastic rotations of above 25 mrad, indicating that these steel connections conform with the minimum European requirements for ductility class medium. Ultimately, the numerical models were able to capture the local effects, as well as the key structural response characteristics indicating that the modelling procedures can be employed for further extensive parametric investigations.

ACKNOWLEDGEMENTS

The financial support of the Research Fund for Coal and Steel of the European Community within the projects EQUALJOINTS Grant agreement no. RFSR-CT-2013-00021 and, EQUALJOINTS-PLUS Grant agreement no 754048 (2017) for the tests and numerical investigations in this paper are gratefully acknowledged.

REFERENCES

[1] Plumier A., New idea for safe structures in seismic zones, *IABSE Symposium: Mixed structures including new materials*, Brussels, 1990. p. 431-6. doi:10.5169/seals-46518

[2] N.R. Iwankiw C.J. Carter, Dogbone: a new idea to chew on, *Modern Steel Construction*, pp. 18-26, April 1996.

[3] M.D. Engelhart, T. Winneberger, A.J. Zekany, T.J. Potyraj, The dogbone connection: part 2 Selectively trimming a portion of a beam allows connection strength to exceed beam strength without the need to develop a stronger connection, *Modern Steel Construction*, 1996.

[4] A. Zekioglu, H. Mozaffarian, K. Le Chang, C.M. Uang, Designing after Northridge: a California engineering firm re redesigned a project's connections to ensure adequate seismic performance, *Modern Steel Construction*, March 1997.

[5] E. P. Popov, T.S. Yang, S.P. Chang, Design of steel MRF connections before and after 1994 Northridge earthquake, *Engineering Structures*, **20(12)**, 1030–1038, 1998 doi:10.1016/S0141-0296(97)00200-9

[6] C.M. Uang, C.C, Fan., Cyclic stability criteria for steel moment connections with reduced beam section, *Journal of Structural Engineering*, **127(9)**, 1021-1027, 2001. doi:10.1061/(ASCE)0733-9445(2001)127:9(1021)

[7] X. Zhang, J.M. Ricles, Seismic Behavior of Reduced Beam Section Moment Connections to Deep Columns, *Journal of Structural Engineering*, **132(3)**, 358-367, 2006. doi:10.1061/(ASCE)0733-9445(2006)132:3(358)

[8] X. Zhang, J.M. Ricles, Experimental Evaluation of Reduced Beam Section Connections to Deep Columns, *Journal of Structural Engineering*, **132(3)**,346-357, 2006. doi:10.1061/(ASCE)0733-9445(2006)132:3(346)

[9] ANSI 360-16, *AISC: Specification for Structural Steel Buildings*, 2016, Chicago, IL

[10] ANSI 341-16, *AISC. Seismic Provisions for Structural Steel Buildings*, 2016, Chicago, IL

[11] ANSI 358-14, *AISC: Prequalified Connections for Special and Intermediate Steel Moment Frames for Seismic Applications*, 2014, Chicago, IL

[12] L. Qi, J. Paquette, M. Eatherthon, R. Leon, T. Bogdan, N. Popa, E. Nunez Moreno, Analysis of Fracture Behaviour of Large Steel Beam Column Connections, *12th International Conference on Advances in Steel-Concrete Composite Structures (ASCCS)*, 2018 doi:10.4995/ASCCS2018.2018.7122

[13] R. Landolfo, M. D'Aniello, S. Costanzo, R. Tartaglia, A. Stratan, D. Dubina, C. Vulcu, C. Maris, C. Zub, L. Da Silva, C. Rebelo, H. Augusto, A. Shahbazian, F. Gentili, J.P. Jaspart, J.F. Demonceau, L.V. Hoang, A.Y. Elghazouli, A. Tsitos, O. Vassart, E. Moreno Nunez, V. Dehan, C. Hamreza, *European pre-QUALified steel JOINTS (EQUALJOINTS)*, Final Report, 2018-05-04, Directorate-General for Research and Innovation (European Commission). 2018 Available from: https://publications.europa.eu/s/j7q0 [Accessed 7th January 2019]

[14] DSS (Dassault Systèmes Simulia Corp). *ABAQUS Analysis user's manual 6.14-2*, DSS, Providence, RI, USA. 2014

[15] D.V. Bompa, A.Y. Elghazouli, Numerical modelling and parametric assessment of hybrid flat slabs with steel shear heads, *Engineering Structures*, **142**, 67-83, 2017. doi:10.1016/j.engstruct.2017.03.070

[16] H. Augusto, L. Simões da Silva, C. Rebelo, J.M. Castro, Cyclic behaviour characterization of web panel components in bolted end-plate steel joints. *Journal of Constructional Steel Research*, **133**, 310-333, 2017. doi:10.1016/j.jcsr.2017.01.021.

[17] J.M. Castro, F.J. Dávila-Arbona, A.Y. Elghazouli. Seismic design approaches for panel zones in steel moment frames. *Journal of Earthquake Engineering*, **12**, 34-51, 2008. doi:10.1080/13632460801922712.

[18] J.M. Castro, A.Y. Elghazouli, B.A. Izzuddin. Modelling of the panel zone in steel and composite moment frames. *Engineering Structures*, **27(1)**, 129-144, 2005. doi:10.1016/j.engstruct.2004.09.008.

[19] CEN (European Committee for Standardisation), *EN 1998-1, Eurocode 8: Design of structures for earthquake resistance - Part 1 : General rules, seismic actions and rules for buildings*, Brussels, 2004